Polymer Testing 145 (2025) 108746

Contents lists available at ScienceDirect

Polymer Testing

journal homepage: www.elsevier.com/locate/polytest

Analysis of covalent adaptable networks Based on disulfide exchange through broadband dielectric spectroscopy

B. Pascual-Jose [a], R. Teruel-Juanes [a], S. de la Flor [b], A. Serra [c], A. Ribes-Greus [a,*]

[a] Research Institute for Materials Technology (IUTM), Universitat Politècnica de València (UPV), Camí de Vera, s/n, 46022, Spain
[b] Department of Mechanical Engineering, Universitat Rovira i Virgili (URV), 43007 Tarragona, Spain
[c] Department of Analytical and Organic Chemistry, Universitat Rovira i Virgili (URV), 43007 Tarragona, Spain

ARTICLE INFO

Keywords:
Disulfides
Covalent adaptable networks
Vitrimers

ABSTRACT

To study the nature and the cooperativity of the disulfide exchange mechanism in covalent adaptable networks, the dielectric and conductive properties of three membranes obtained by curing diglycidyl ether of bisphenol A (DGEBA) with hexamethylenediamine (HMDA), cystamine (CYS), or a mixture of both diamines in the same proportion were studied. Significant differences in the dielectric relaxation spectra of the three membranes were observed. In the low-temperature region, the dielectric spectra displayed two non-cooperative dielectric relaxations (γ and β). In the DGEBA/HMDA-CYS membrane, its relaxation function and activation energy are between those corresponding to the DGEBA/HDMA and DGEBA/CYS membranes, but their relationship does not depend linearly on the composition. In the high-temperature region, a dielectric relaxation of cooperative origin related to the glass transition (α) was observed in the membrane cured with hexamethylenediamine. However, the relaxation related to the glass transition overlaps with the exchange of the disulfide bonds in the membranes with cystamine. The analysis of the electric conductivity (σ) reveals an abrupt increment that suggests a radical-mediated dissociative bond exchange reaction may be occurring. However, the analysis of the σ_{DC} curves is indicative of an associative bond exchange reaction. The rapid formation of new associations among radicals is proposed to explain the vitrimer-like behaviour on these CYS-containing membranes.

1. Introduction

Among the different existing thermosets, epoxy resins are an important class given some outstanding properties such as dimensional and thermal stability, mechanical strength, electric insulation, and chemical resistance. This is why they are widely used in different fields, such as aerospace, transportation architecture, and electronics [1,2]. Due to the diverse operating conditions in each field, epoxy materials can suffer serious mechanical damage, creep, cracks, fractures, etc., due to the enormous stresses they undergo, which undermine their service lifetime, resulting in waste. An important effort is put into producing optimal epoxies that exhibit recyclable, healable, and reprocessable characteristics. Generally, this is achieved using polymeric networks in which covalent dynamic bonds are introduced. Moreover, in some cases non-covalent interactions can be used to improve these special characteristics, but usually fragile behavior is observed, and therefore, the materials yield under large stresses [3–5].

Disulfide exchange is one of the most extensively used exchangeable groups in the design of covalent adaptable networks (CANs) [6–9]. Currently, disulfide groups are garnering significant interest due to their rapid stress relaxation times and their ease of recycling, both mechanically and chemically [10].

Several mechanisms have been suggested to explain how disulfides introduce reversibility into a polymer network, including a) disulfide metathesis, b) radical-mediated exchange, and c) thiol-disulfide exchange, as it is represented in Scheme 1 [11,12].

Among these mechanisms, the radical-mediated pathway is regarded as the most likely in aromatic disulfide moieties. Through Electron Spin Resonance (ESR) studies the formation of radicals was detected for bis (4-hydroxyphenyl) disulfide [11]. However, the reaction mechanism can also be influenced by other factors, such as the presence of nucleophiles (e.g., tertiary amines or phosphines) that can attack the disulfide bond, producing a thiolate anion that takes part in thiol-disulfide exchange reactions [12–14]. This mechanism may become more dominant when thiols are present in excess as curing agents or when there is a high concentration of tertiary amines in the network. The radical-mediated

* Corresponding author.
E-mail address: aribes@ter.upv.es (A. Ribes-Greus).

https://doi.org/10.1016/j.polymertesting.2025.108746
Received 5 November 2024; Received in revised form 24 February 2025; Accepted 25 February 2025
Available online 26 February 2025
0142-9418/© 2025 The Authors. Published by Elsevier Ltd. This is an open access article under the CC BY-NC-ND license (http://creativecommons.org/licenses/by-nc-nd/4.0/).

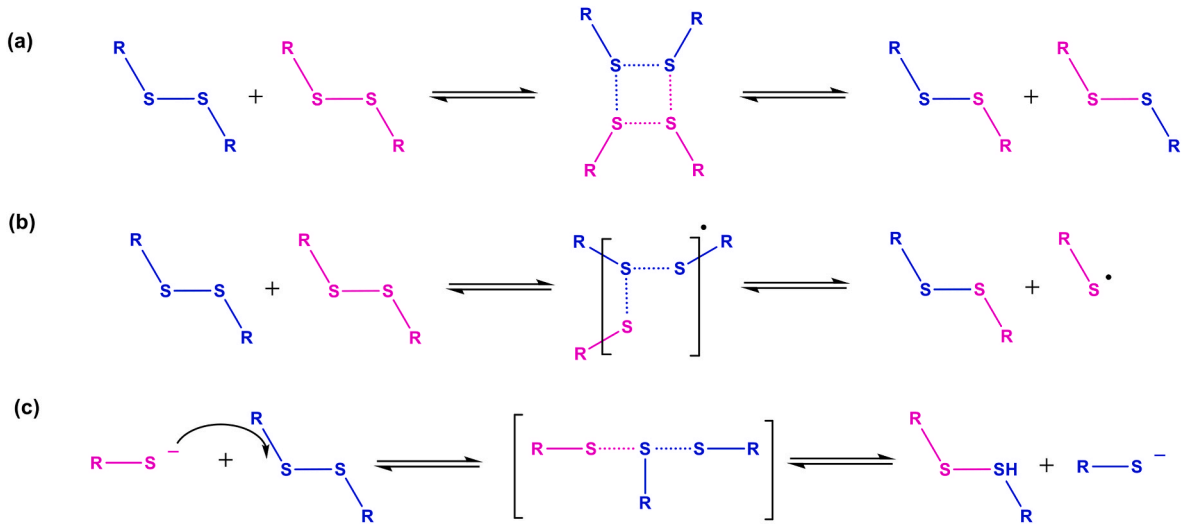

Scheme 1. Proposed mechanisms for disulfide exchange: a) disulfide metathesis, b) radical-mediated exchange, and c) thiol-disulfide exchange.

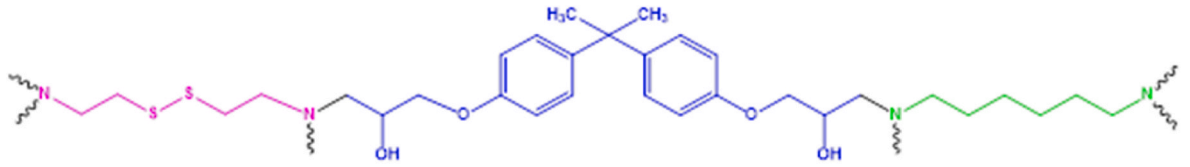

Scheme 2. Constitutive units of the network structure derived from: DGEBA (blue), HMDA (green) and CYS (pink) in the membrane DGEBA/HMDA-CYS.

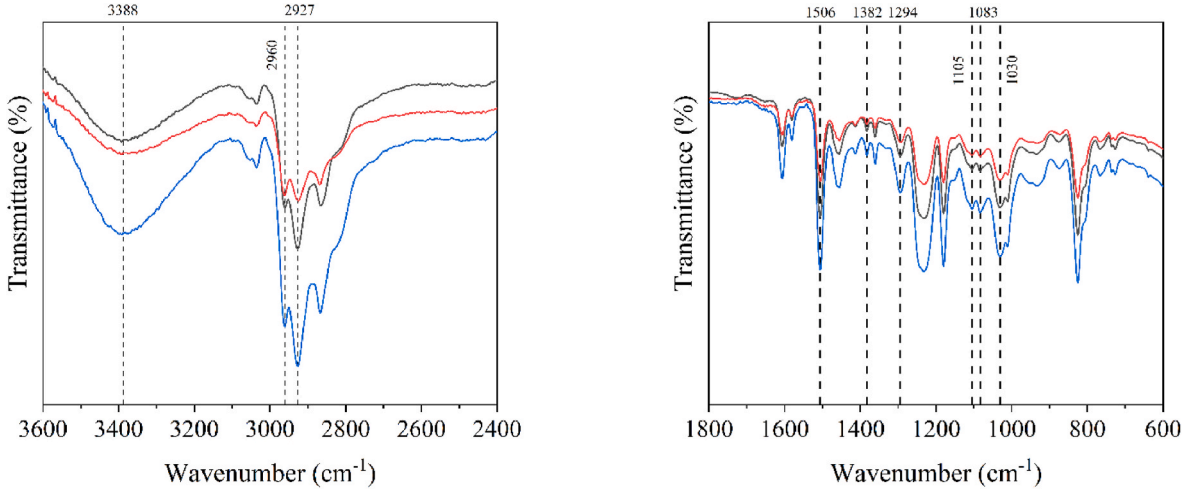

Fig. 1. Stacked FTIR spectra for the DGEBA/HMDA (black line), DGEBA/HMDA-CYS (blue line), and DGEBA/CYS (red line) membranes.

pathway indicates a dissociative mechanism, whereas the catalyzed thiol-disulfide exchange suggests an associative mechanism and this type of material falls in the definition of vitrimers [15]. Consequently, in the absence of nucleophiles, a reduction in network integrity might be anticipated. However, the reverse reaction, which forms new disulfide bonds, occurs quickly enough to classify these materials as vitrimer-like. This behavior can be observed macroscopically, as there is no abrupt decrease in viscosity, exhibiting a physical behavior consistent with associative mechanisms, following an Arrhenius relationship [16].

The relaxation behavior is affected by nearby substituents on the disulfide, which influences both the strength of the S-S bond and the stability of the resulting radicals. Luzuriaga et al. observed variations in relaxation rates between 2-aminophenyl disulfide and 4-aminophenyl disulfide curing agents [17]. They found that amine groups in the ortho position lower the dissociation energy of the disulfide, promoting the formation of thiyl radicals. As a result, variations in reactivity can be expected between aromatic and aliphatic disulfides, making experimental mechanistic studies particularly motivating.

Broadband dielectric spectroscopy (BDS) is a well-established method for investigating the dynamics of polymers by examining their response to an electrical perturbation across a wide range of frequencies and temperatures. This approach yields valuable information about large supramolecular systems and molecular motions. While its application to the analysis of CANs is not extensive [18,19], BDS has the potential to provide important insights into the bond exchange mechanism. Thus, BDS can deliver valuable information across a wide range of temperatures and frequencies, which could be crucial for the physical and mechanistic characterization of CANs.

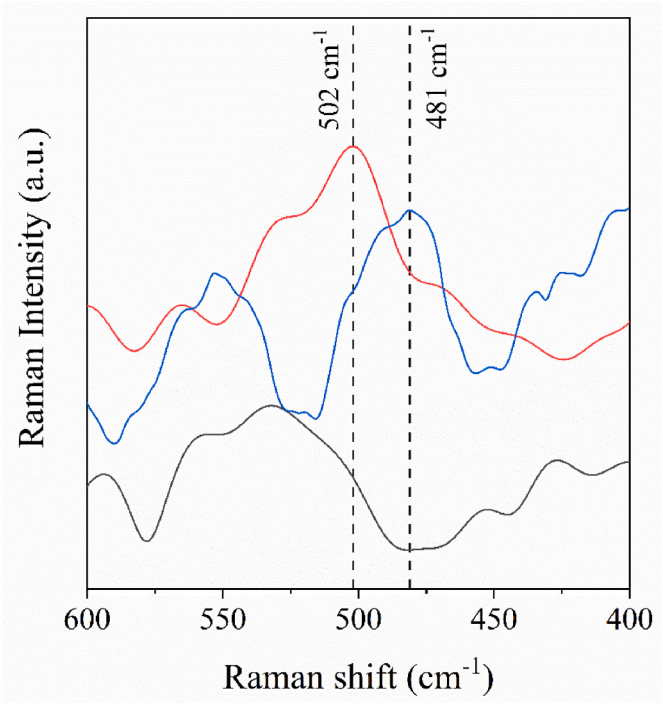

Fig. 2. Ramman spectra for the DGEBA/HMDA (black line), DGEBA/HMDA-CYS (blue line), and DGEBA/CYS (red line) membranes.

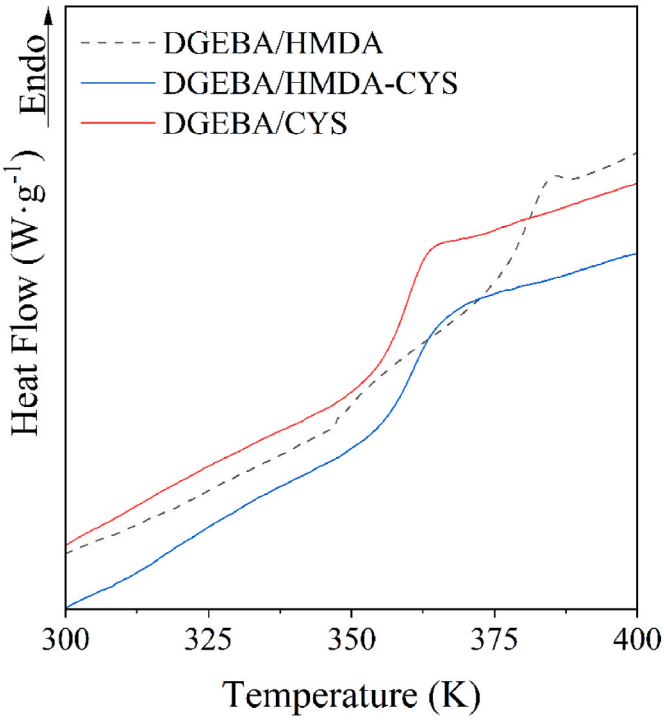

Fig. 3. DSC thermograms of the 2nd Heating for all the studied membranes.

The present study characterizes disulfide CANs by examining their dielectric and conductive properties. Additionally, the characterization includes an analysis of the chemical structure using Fourier transform infrared spectroscopy (FTIR) and Raman spectroscopy and an assessment of thermal properties through differential scanning calorimetry (DSC). The dielectric relaxation spectrum is thoroughly analyzed to gain insight into molecular dynamics, particularly the molecular motions involving dynamic disulfide bonds. Electric conductivity is also analyzed to determine whether the bond exchange mechanism is associative or dissociative. In this study, three different DGEBA membranes are examined: the first cured with hexamethylene diamine (HMDA), the second with cystamine (CYS), and the third using an equimolecular ratio of both amines. The stoichiometric epoxy/amine molar ratio of 2:1 has been maintained in all membranes.

The difficulty of directly measuring the topological freezing temperature (T_v), the temperature below which the vitrimer network structure becomes effectively rigid and significantly restricts molecular mobility, has been previously addressed [20]. This challenge is influenced by factors such as the density of exchangeable cross-links, the kinetics of the exchange reactions, the mobility of the polymer chains, and the availability of reactive chemical functions. Therefore, BDS can be a valuable tool for determining T_v.

2. Experimental procedure and calculations

2.1. Materials

Diglycidyl Ether of Bisphenol A (DGEBA) trade name ARALDITE GY240, 5.51 eq/kg was a gift from Huntsman. Hexamethylenediamine (HMDA, 116.21 g/mol, M_p: 39-42 °C) and cystamine dihydrochloride were obtained from Merck. Previously to be used as curing agent cystamine hydrochloride was neutralized with a 3 M sodium hydroxide solution and extracted with ethyl acetate to obtain the free base (CYS, 152.28 g/mol, M_p: 135-6 °C).

Stoichiometric proportions of DGEBA and the appropriate curing agent were mixed, then degassed under vacuum at 40 °C. The mixture was poured into an open metal mold with a Teflon separator of approx. 1 mm and cured in the oven for 3 h at 100 °C, 2 h at 150 °C, and 2 h at 180 °C to achieve complete curing. The curing schedule was optimized to reach the maximum T_g. The membranes were labelled DGEBA/HMDA, DGEBA/CYS and DGEBA/HMDA-CYS, respectively.

2.2. Fourier transformed infrared spectroscopy (FTIR)

The chemical structure was assessed through Fourier Transform Infrared Spectroscopy (FTIR). Analyses were carried out in a Thermo Nicolet 5700 infrared spectrometer with an attenuated total reflectance accessory (ATR). The spectra were collected from 4000 to 400 cm^{-1} at a resolution of 4 cm^{-1} along 64 scans. The spectra of three different locations of the membrane were averaged. Backgrounds were collected, and results were processed through the Omnic® Software.

2.3. Raman spectroscopy

The chemical structure was also assessed through Raman spectroscopy. Analyses were carried out using a Thermo Fischer Scientific Nicolet iS50 Raman spectrometer. The spectra were collected from 4000 to 400 cm^{-1} at a resolution of 32 cm^{-1} along 64 scans. Results were processed through the Omnic® Software.

2.4. Differential scanning calorimetry (DSC)

The differential scanning calorimetry (DSC) analyses were evaluated using Mettler Toledo DSC822e equipment. Aluminium capsules were filled with 2 and 4 mg of the membranes and sealed. Then, they were subjected to a heating/cooling program with a rate of 5 °C·min^{-1} over the 248K–523K temperature range under an inert atmosphere with a flow rate of 50 mL min^{-1} of nitrogen.

2.5. Broadband dielectric spectroscopy (BDS)

The impedance measurements were conducted using a Novocontrol Broadband Dielectric Impedance Spectrometer (BDIS) connected to a

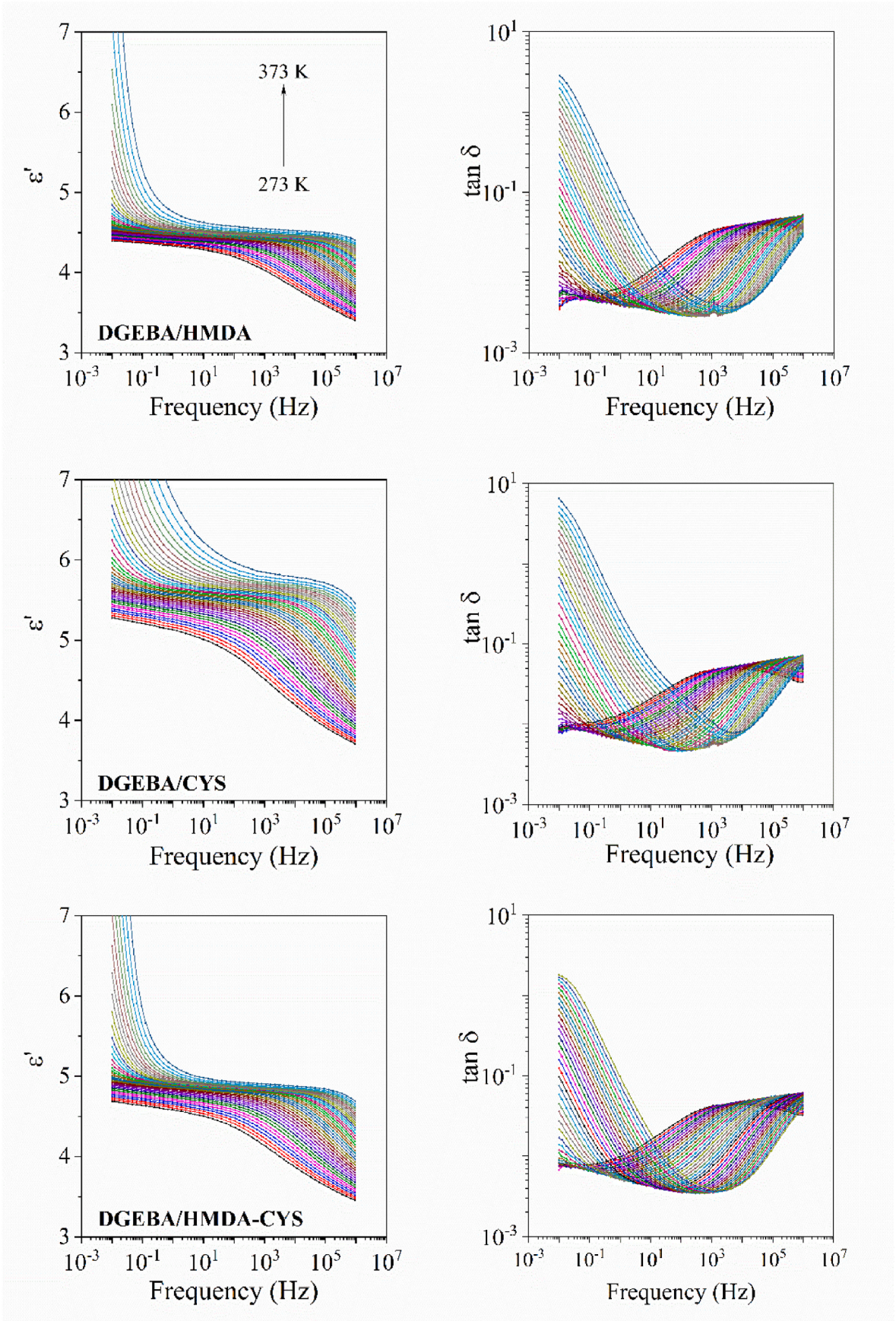

Fig. 4. Isothermal plots of the real (ε′) part of the complex permittivity (ε*) and loss tangent (tan δ) for the DGEBA-CYS, DGEBA/HMDA-CYS, and DGEBA/HMDA membranes in the temperature range from 273 to 373K.

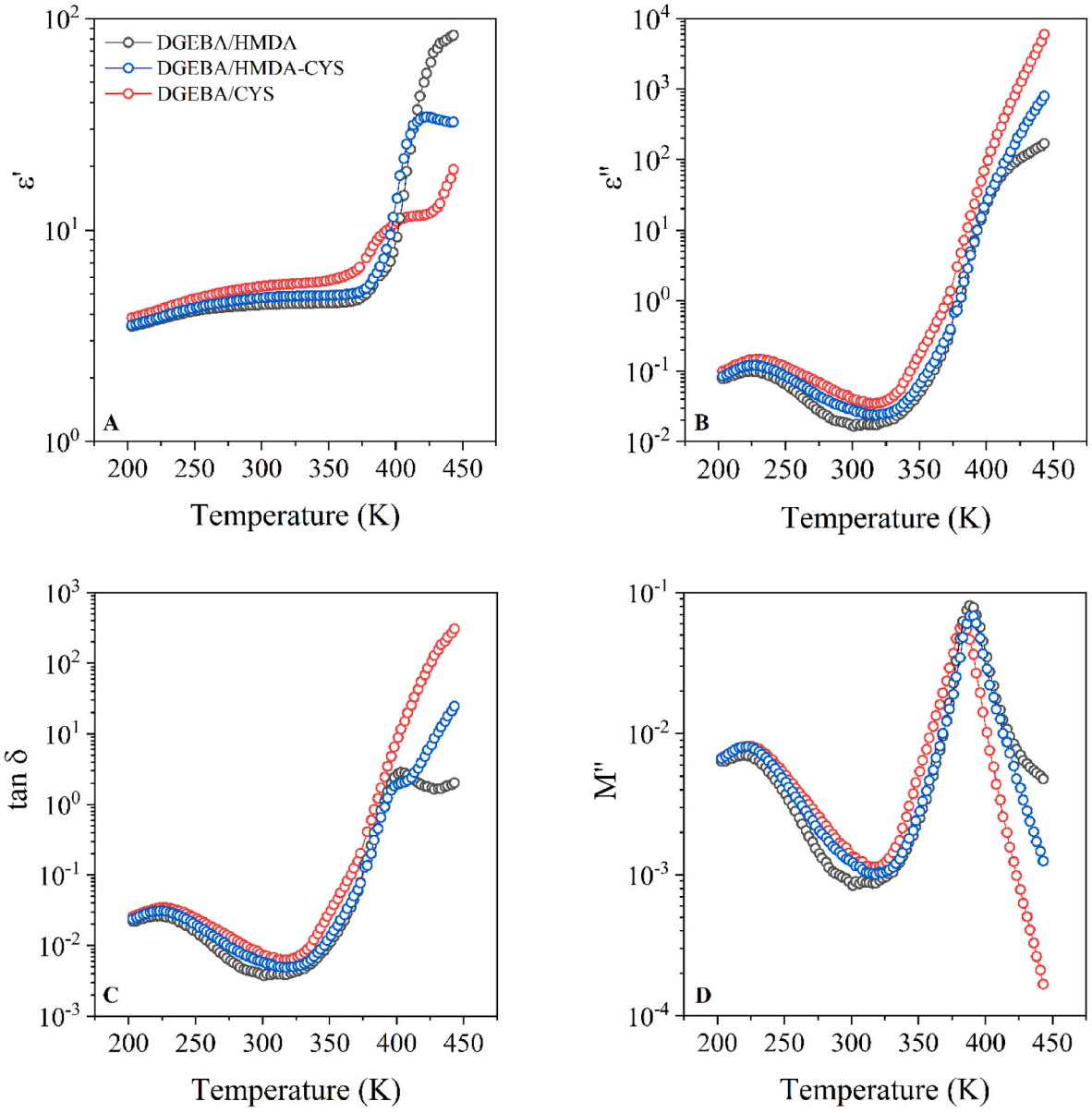

Fig. 5. Isochronal curves for A) the real part of the dielectric permittivity (ε′), B) the imaginary part of the dielectric permittivity (ε″), C) the tan δ, D) the imaginary part of the electric modulus (M″) for the DGEBA-CYS, DGEBA/HMDA-CYS, and DGEBA/HMDA membranes at a frequency of 1 Hz.

Novocontrol Alfa-A Frequency Response Analyzer. The measurements were run in the frequency range of 10^{-1} to 10^{-7} Hz at the temperature range 203K–443K. All the measurements were performed under isothermal conditions by increasing steps by 2.5K. Thus, a better resolution of every dielectric process can be obtained. The membrane electrode assembly (MEA) consisted of two stainless steel electrodes filled with the membrane. Consequently, the resulting MEA was directly placed in the cell. The dielectric spectra were analyzed in terms of the complex permittivity (ε*) [21]. All the characteristic parameters of each relaxation process were determined as shown in equation (1):

$$\varepsilon^{*}(\omega) = \varepsilon_{\infty} + \frac{\Delta\varepsilon}{(1 + (i\omega\tau_i)^{\alpha_i})^{\beta_i}} \quad (1)$$

Where τ_i is the Havriliak-Negami (HN) relaxation time, α_i and β_i are parameters corresponding to the width and asymmetry of the relaxation peak, respectively. $\Delta\varepsilon$ is the value of the relaxation strength. Note that at each isothermal curve of ε* there are more than one dielectric process, and thus a maximum of three dielectric processes are used for the fitting, i.e., one for the main segmental relaxation and two for the secondary ones.

The analysis of the temperature dependence of the relaxation times is shown in equations (2)–(4). Accordingly, if a linear relationship is obtained the Arrhenius equation is used. On the other hand, if the relationship is nonlinear the Vogel-Fulcher-Tamman-Hesse (VFTH) equation is utilised [22].

$$f_{max} = f_0 \exp\left(\frac{-E_a}{RT}\right) \quad (2)$$

$$\tau(T) = \tau_0 \exp\left(\frac{B}{T - T_{VFTH}}\right) \quad (3)$$

$$E_{a(T_g)} = \frac{RB}{\left(1 - T_0/T_g\right)^2} \quad (4)$$

Where f_{max} refers to the maximum frequency, τ is the relaxation time, f_0

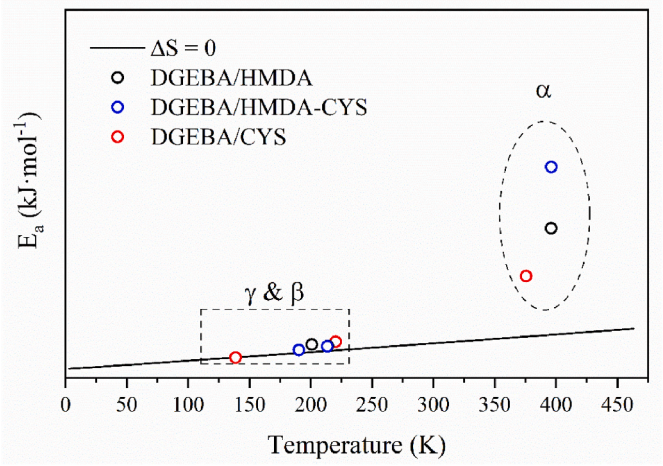

Fig. 6. Eyring map for the DGEBA/CYS, DGEBA/HMDA, and DGEBA/HMDA-CYS membranes.

and τ_0 are pre-exponential terms, $B = D{\cdot}T_{VFTH}$ is an activation parameter where D refers to the fragility, and T_{VFTH} is the temperature obtained from the best fit of the VFTH equation. T_g is the glass transition temperature, E_a is the activation energy, and R is the ideal gas constant.

The response to an applied electric field of a polymer consists mainly of frequency-dependent and frequency-independent components. The former is ascribed to the DC conductivity and shows a frequency-independent plateau. In contrast, the latter is attributed to the AC conductivity and is characterised by a high dispersion at higher frequencies. This behaviour can be modelled by Jonscher's power law [21], as shown in Equation (5):

$$\sigma(\omega) = \sigma_{DC} + \sigma_{AC} = \sigma_{DC} + A\omega^n \tag{5}$$

Where A is the pre-exponential factor, σ_{DC} is the frequency-independent value, and n is the fractional exponent varying between 0 and 1.

3. Results

3.1. Chemical structure

The curing reaction of DGEBA with aliphatic primary amines leads to well-defined structures with β-hydroxyamine groups by the attack of the nucleophilic amine to the methylene carbon of the epoxy group. The structure of the network is depicted in Scheme 2.

The chemical structure of the network was confirmed by FTIR and Raman spectroscopy. The most characteristic peaks in the FTIR for the three membranes prepared are shown in Fig. 1.

The most significant observation is the complete disappearance of the epoxide absorption at 915 cm^{-1}, indicating that the fully cure has been achieved. In the spectra we can see the bands at 1030 cm^{-1} (δ C-H of the 1–4 substituted benzene and υ_{sym} (C-O-C) bond in the case of the aromatic ether); 1083 cm^{-1} (bending of the C-H bond of the benzenic ring); 1105 cm^{-1} (stretching C-N bond and deformation of geminal methyl groups); 1294 cm^{-1} (twisting and wagging of the CH_2 group, bending of OH groups); 1382 cm^{-1} (symmetric in-plane bending vibration of the gem-CH_3 groups) and 1506 cm^{-1} (stretching vibration of C=C bonds in the para-substituted aromatic ring) [23]. The S-S absorptions in the FTIR band are very weak, because of the low dipolar moment and cannot be identified. In contrast, the Raman spectrum can accurately identify the characteristic peak of the disulfide bond.

In Fig. 2, the membranes containing cystamine show the peaks in the characteristic region corresponding to the S-S bonds. Note that in the DGEBA/HMDA-CYS spectrum the characteristic disulfide bond (S-S) peak appears, however, a noticeable displacement is found attributable to changes in dihedral angles [24]. As can be seen, DGEBA/HMDA does not display any peak in this region.

Table 1
Parameters of the Arrhenius equation of the γ-relaxation for all the membranes.

Membrane	E_a (kJ · mol^{-1})	$T_{max,\ 1\ kHz}$ (K)	R^2
DGEBA-CYS	32	187	0.981
DGEBA-HMDA	$E_{a1} = 42$	243	0.751
	$E_{a2} = 68$	253	0.979
DGEBA-HMDA-CYS	$E_{a1} = 73$	243	0.958
	$E_{a2} = 66$	237	0.899

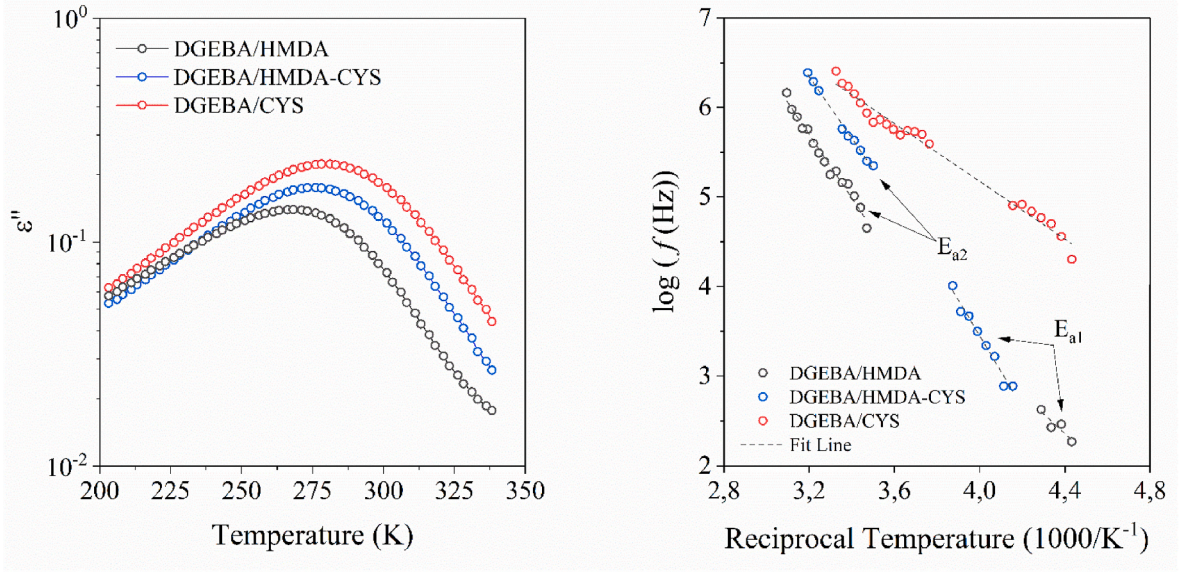

Fig. 7. (Left) Isochronal curves at a frequency of 10^3 Hz; (Right) Arrhenius map for the γ-relaxation for the DGEBA/CYS, DGEBA/HMDA, and DGEBA/HMDA-CYS membranes.

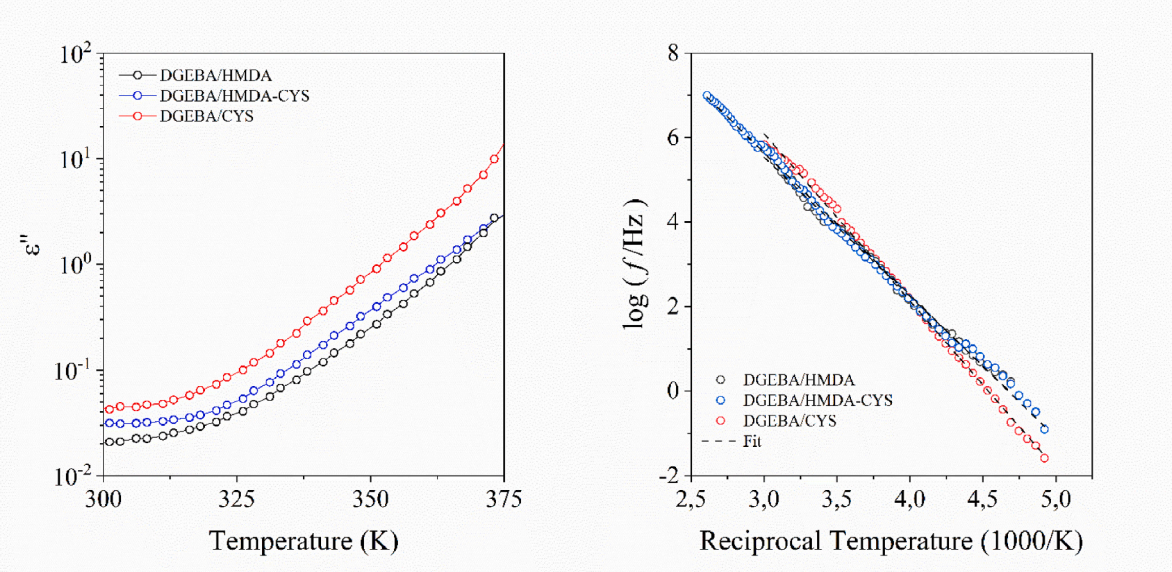

Fig. 8. (Left) Isochronal curves at a frequency of 10^3 Hz; (Right) Arrhenius map for the β-relaxation for the DGEBA/CYS, DGEBA/HMDA, and DGEBA/HMDA-CYS membranes.

Table 2
Parameters of the Arrhenius equation of the β-relaxation for all the membranes.

Membrane	E_a (kJ · mol^{-1})	$T_{max,\ 1\ kHz}$ (K)	R^2
DGEBA-CYS	76	265	0.997
DGEBA-HMDA	63	265	0.995
DGEBA/HMDA-CYS	64	264	0.997

3.2. Thermal analysis

The glass transition temperature (T_g) is important in thermosets. When this temperature is exceeded, the network structure gains increased mobility, causing the material to become rubbery. Its assessment is performed through the differential scanning calorimetry (DSC). T_g was determined by DSC (Fig. 3) and the values are 379 K for the DGEBA/HMDA, 361 K for DGEBA/HMDA-CYS and 358 K for DGEBA/CYS determined using the midpoint.

As observed, the increase in CYS within the membrane leads to a decrease in the T_g value due to the longer S-S and S-C bonds compared to C-C linkages. This enhances the mobility of the CYS moieties, resulting in a lower T_g.

3.3. Analysis of the dielectric spectra

The complex permittivity formalism performs the dielectric response (ε^*). The dielectric spectra have been analyzed in the frequency range ($f = 10^{-2} - 10^7$ Hz) and temperatures from 203 to 443 K, in terms of the real (ε') and imaginary (ε'') parts of complex permittivity, the loss tangent (tan δ), and the imaginary part (M") of the complex electric modulus (M*).

Fig. 4 plots the isothermal curves of ε', and tan δ for all the studied membranes. At sufficient high temperatures and low frequencies, the values of ε', and tan δ rise, exceeding the range typical of dielectric relaxations and suggesting the prevalence of conductivity in that region. At low temperatures and a large range of frequency, dielectric relaxations appear. For the sake of clarity, to distinguish all-dielectric relaxation processes, the isochronal curves of ε' and tan δ at 1 Hz are plotted in Fig. 5. Three dielectric relaxations typical of DGEBA network spectra are found. The dielectric relaxations are labelled as γ, β, and α in order of increasing temperature.

The γ and β relaxations appear at low temperatures and are associated with local mobility of the side chains, exhibiting weaker intensities. At higher temperatures, α relaxation is observed, which is related to the glass transition. As already noted in differential scanning calorimetry results, the glass transition temperature decreases with an increase in cystamine percentage. Some researchers attribute this effect to the disulfide bonds acting as spacers, enhancing intermolecular movement between polymer chains. Indeed, this enhancement of chain mobility has a direct impact on reducing the T_g value, thereby rendering the membrane more flexible and responsive under conditions of lower thermal energy [25–27].

From the point of view of molecular mobility, the cooperativity is evaluated through the Eyring model, as formulated by Starkweather [28,29]. Consequently, E_a values proximal to the zero-entropy line expressed as $E_a = RT[22.92 + \ln T]$ are deemed of intramolecular (or non-cooperative) origin, as the role of entropy can be neglected in this type of molecular relaxation. Conversely, values deviating significantly from the zero-entropy line are categorized as intermolecular (or cooperative) origin, indicating a substantial entropy contribution. Therefore, as illustrated in Fig. 6, both the γ- and β-relaxation exhibit values near the zero-entropy line, suggesting a non-cooperative origin. In contrast, the E_a values corresponding to the α-relaxation lie considerably distant from the zero-entropy line, and thus a cooperative origin is ascribed. In Addition, this result confirms the spacer effect of the disulfide group. When the percentage of cystamine increases, the number of disulfide groups that facilitate intermolecular movement increases, and thus the glass transition temperature decreases.

To better understand the observed dielectric relaxations, it's important to look at how relaxation times change with temperature. For clarity, the spectrum has been divided into two zones, each reflecting the macromolecular movements involved.

3.3.1. Analysis of the low-temperature region

In the low-temperature range, the γ- and β-relaxations appear in order of increasing temperature. Despite assigning these relaxations to intramolecular motion, the macromolecular origin of the γ-relaxation is still debated, with two prevailing theories. Some researchers attribute this molecular motion to unreacted moieties, particularly epoxide groups within the system. Conversely, others suggest that this molecular motion is associated with the local movements of backbone sequences, specifically methylene sequences, including ether groups [30,31].

The differences observed among the three membranes in the

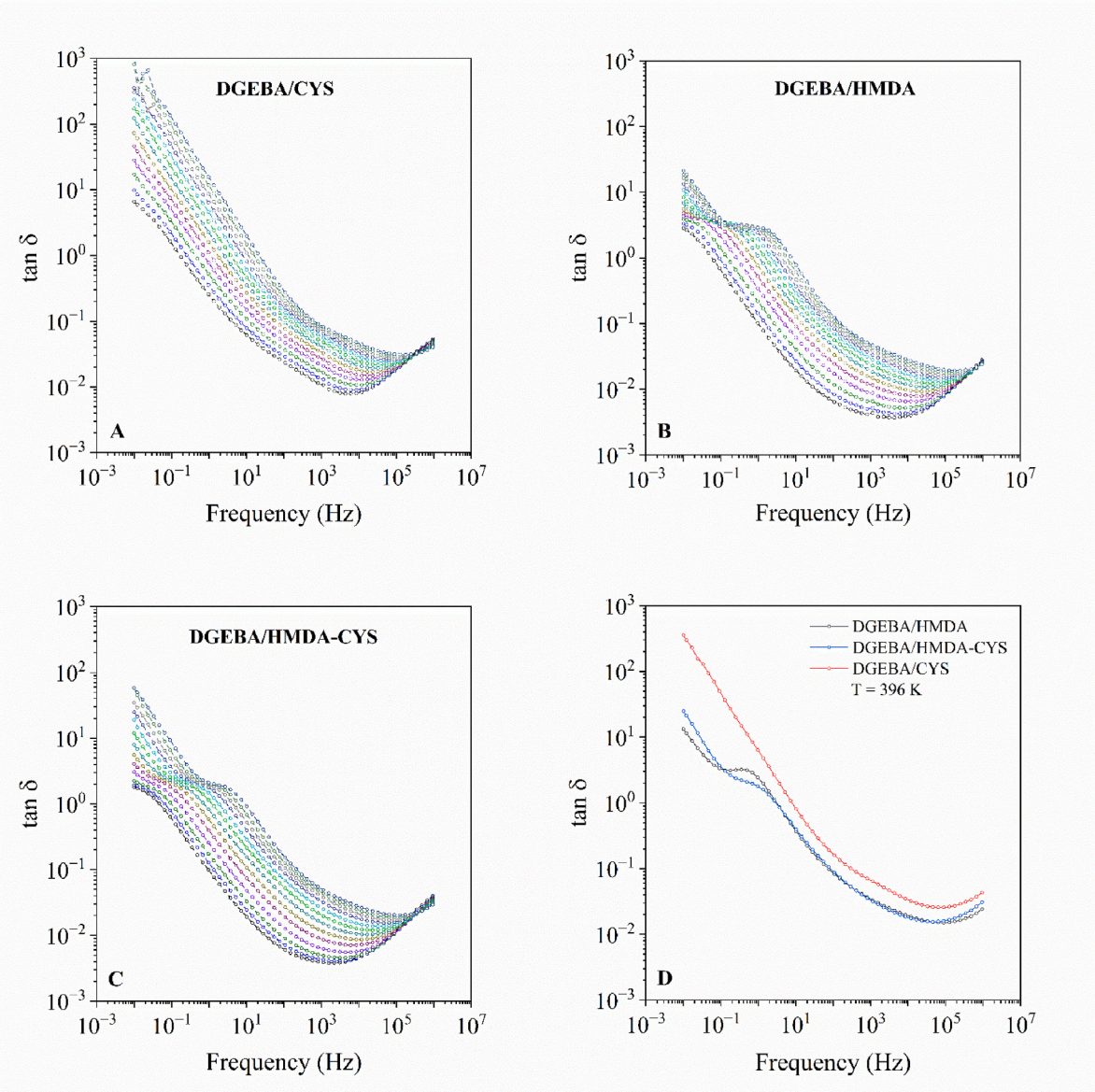

Fig. 9. Isothermal plots of loss tangent (tan δ) for the (A) DGEBA/CYS, (B) DGEBA/HMDA, (C) DGEBA/HMDA-CYS membranes; (D) Detailed view at 396 K.

Arrhenius plot indicate that the molecular origin is related to its final structure rather than to unreacted moieties. It is evident that the differences correlate with the proportion of CYS in the membrane formulation. Therefore, the relationship between relaxation times and temperature in membrane cured with HMDA-CYS reflects the contributions of both curing agents. At lower temperatures, DGEBA/HMDA-CYS behaves similarly to DGEBA/HMDA, while at higher temperatures, its behavior falls between both DGEBA/CYS and DGEBA/HMDA.

The Arrhenius plot for the γ-relaxation is displayed in Fig. 7. All the membranes are fitted by means of an Arrhenius model provided its non-cooperative nature. The results of apparent activation energy are gathered in Table 1.

Fig. 7 also shows a dispersion in the relationship between relaxation times and temperature. The activation energy value (E_a) for the DGEBA/CYS membrane is lower than (E_{a2}) for the DGEBA/HMDA, while DGEBA/HMDA-CYS falls in between. The DGEBA/CYS exhibits a characteristic activation energy (E_a) value for the dielectric process, whereas DGEBA/HMDA and DGEBA/HMDA-CYS exhibit higher values. This finding aligns with results from previous works [32].

At elevated temperatures, β-relaxation is observed. Fig. 8 displays the Arrhenius plot for this process, which is typically linked to the local rotational motion of pendant hydroxyl groups in relation to the chain backbone [30,33]. The analysis of the relaxation times as a function of the temperature follows the Arrhenius model, with the fitting parameters summarized in Table 2. The observed apparent activation energy values align with previous research findings [31,32].

The results indicate that the disulfide group in CYS does not significantly affect the temperature peak of β-relaxation. In contrast, only the DGEBA/CYS membranes exhibit a higher activation energy compared to both the DGEBA/HMDA and DGEBA/HMDA-CYS, which show similar values. The elevated apparent activation energy observed may be influenced by the exchange of disulfide bonds within the membrane, as this process can overlap with both β-relaxation and the glass transition, leading to increased apparent activation energy for the former and decreased values for the latter.

3.3.2. *Analysis of the high-temperature region*

The α-relaxation is associated with the long-range cooperative motion of chains occurring at the glass transition temperature [30,31,33,34]. In this study, we investigated how varying proportions of CYS affect

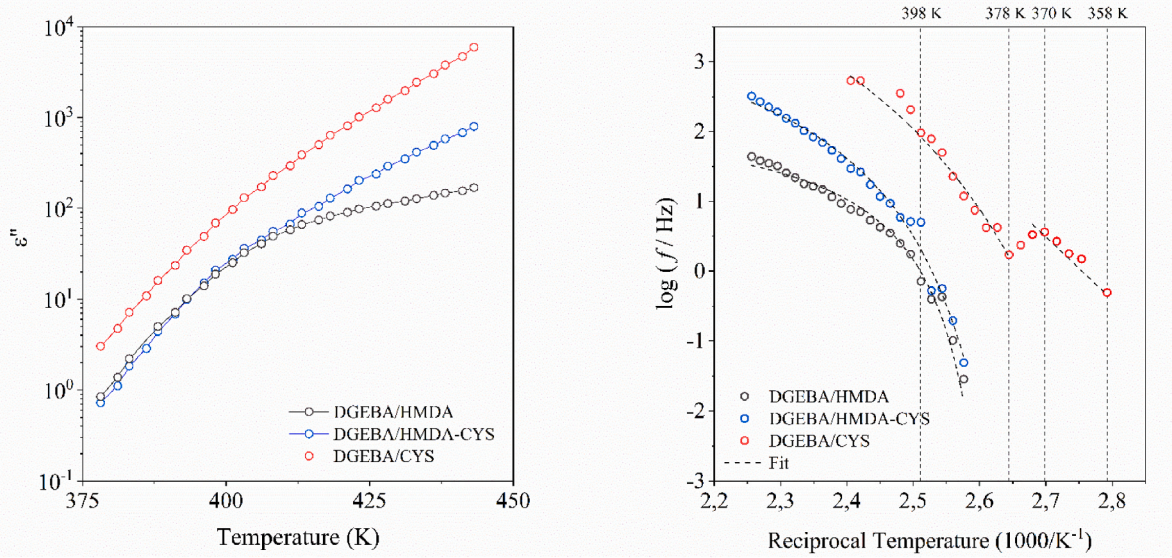

Fig. 10. (Left) Isochronal curves at a frequency of 10^3 Hz; (Right) Arrhenius map for the high-temperature region for the DGEBA/CYS, DGEBA/HMDA, and DGEBA/HMDA-CYS membranes.

Table 3
Parameters of the VFTH equation of the α-relaxation of all the membranes.

Membrane	Log f_0 (Hz)	D	T_{VFTH}	E_a (kJ/mol)	R^2
DGEBA-CYS	6.35	2.24	326.60	259	0.974
DGEBA-HMDA	2.26	0.31	376.01	563	0.987
DGEBA/HMDA-CYS	4.01	0.79	364.21	392	0.986

relaxation times. Fig. 9 illustrates the overlap between the exchange of disulfide bonds and the α-relaxation. Additionally, results also indicate that higher concentrations of disulfide bonds accelerate the relaxation process. Furthermore, a significant increase in conductivity within this temperature range suggests the presence of S radicals, which could be indicative of an ongoing dissociative cleavage reaction (Scheme 1b). This observation supports the hypothesis that the membrane may exhibit vitrimer-like behavior.

Fig. 10 presents the Arrhenius plot and the α-relaxation and the process of the cleavage of the disulfide bonds are observed. It clearly shows that the DGEBA-CYS membrane has two processes or molecular motions overlapped, as mentioned above. One process related to the molecular motion produced by the cleavage of the disulfide bond, and the other related to the cooperative motion of the glass transition, which produced the α-relaxation. In the DGEBA/CYS membrane, a significant proportion of disulfide bonds are present in the membrane, which results in a notable degree of relaxation occurring rapidly.

Conversely, the DGEBA/HMDA membrane lacks disulfide bonds in its microstructure, and the presence of nitrogens extends the temperature range of the α-relaxation. Indeed, in the DGEBA/HMDA-CYS membrane, where cystamine and HMDA are present in equal proportions, the relationship between relaxation time and temperature reflects the effect of both curing agents, indicating that despite a high concentration of internal tertiary amines, the relatively low amount of disulfide bonds is enough to diminished relaxation time. It is not rapid due to the relatively lower percentage of disulfide bonds. However, compared to the α-relaxation exhibited by the DGEBA/HMDA membrane, is evident in the presence of disulfide bonds.

Analysing each of these molecular movements separately, the α-relaxation is a cooperative motion, and the temperature dependence of the α-relaxation is assessed using the Vogel-Fulcher-Tamman-Hesse (VFTH) model. The fitting values are summarized in Table 3. It is obvious that the exchange of the disulfide bonds has an important effect on the cooperative motions that give rise to the glass transition.

Fig. 10 shows the molecular motion produced by the exchange of the disulfide bond have a linear relationship between the relaxation time and the temperature. Consequently, an estimation of the apparent activation energy is performed through an Arrhenius model, and the obtained value is 259 kJ mol^{-1}.

In CANs, another important temperature is the topology freezing temperature (T_v), defined as the temperature at which the material attains a viscosity of 10^{12} Pa s. This temperature is usually determined from an Arrhenius plot or creep experiments [15,20]. T_v indicates the temperature below which chemical exchanges become negligible and can be used to compare bond exchange capabilities in CANs. When T_v is lower than T_g, the T_g becomes the critical factor influencing relaxation behavior. In the glassy state, the lack of segmental motions hampers the occurrence of exchange reactions [35]. The Arrhenius map seems to indicate the temperature range at which the exchange of the disulfide bonds occurs, which depends on the concentration of cystamine present in the membrane.

Accordingly, when the CYS concentration is lower (DGEBA/HMDA-CYS membrane), the temperature at which disulfide bond exchange occurs appears to be higher, and it is overlapped with cooperative motion. These findings correlate with those shown in Fig. 6. In the study by Roig et al. [10], T_v values were determined to be around 343 K, depending on the weight proportion of cystamine and tertiary amines in the membrane.

Concerning the topological freezing temperature (T_v), it is important to highlight that disulfide bonds can undergo the bond exchange reaction through two mechanisms: bond metathesis, characterized by an associative nature, and bond breakage, exhibiting a dissociative nature.

A study by Krouse et al. investigated the relationship between ionic conductivity and medium viscosity in an epoxy/amine formulation during curing. The findings revealed that ion mobility, rather than the number of mobile charge carriers, is the key factor influencing conductivity. This suggests a strong correlation between ion mobility and viscosity changes due to temperature or network growth. Consequently, ionic conductivity measurements might be used to determine whether the molecular exchange mechanism in covalent adaptable networks are dissociative or associative in nature [18,36–38].

3.3.3. *Analysis of the electric conductivity*

The isothermal curves illustrating the real part (σ′) of the complex

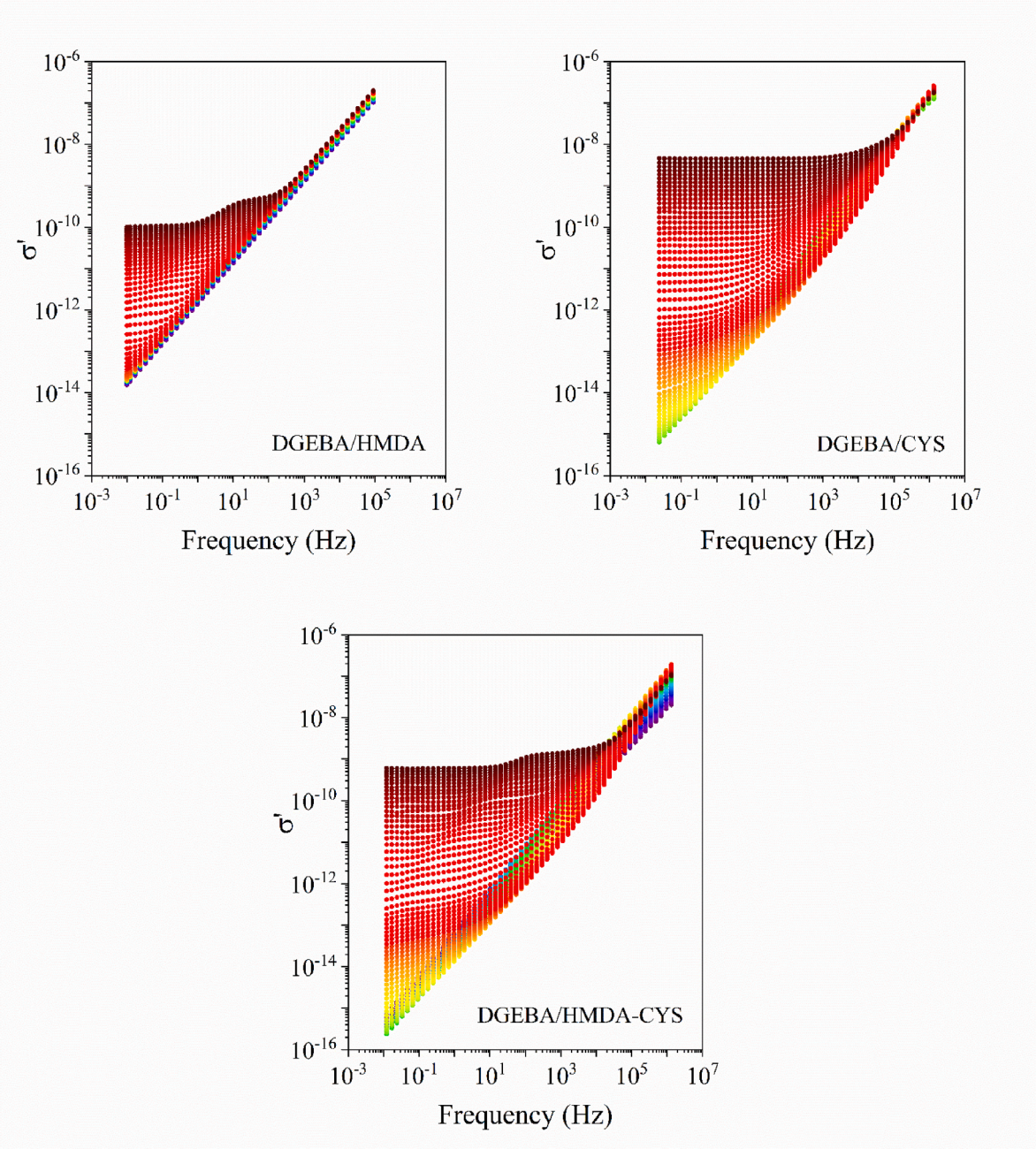

Fig. 11. Isothermal curves of the real part (σ′) of the complex conductivity (σ*) for the DGEBA/CYS, DGEBA/HMDA, and DGEBA/HMDA-CYS membranes.

conductivity (σ*) are depicted in Fig. 11 across the entire temperature range. A clear distinction is observed between the membranes incorporating cystamine and HMDA as curing agents.

In the DGEBA/CYS membrane, the plateau corresponding to DC conductivity is reached at lower temperatures, and as temperature raises, a linear increased is observed, which might be attributed to the cleavage of the disulfide bonds, that overlaps the coupling between the electric conductivity (σ) and the α dielectric relaxation. However, in the DGEBA/HMDA membrane, this coupling between σ and the α dielectric relaxation is clearly visible. In the case of the DGEBA/HMDA-CYS membrane, both phenomena are observed, which agrees with the results illustrated in Fig. 9.

Jonscher's model is employed to ascertain the direct current conductivity (σ_{DC}). Concerning σ_{DC}, the values obtained vary depending on the membrane considered, but the common trend is that in all cases the values increment with increasing temperature, thereby providing evidence for a thermally activated process, as depicted in Fig. 12A. Moreover, the *n*-parameter, serving as a qualitative indicator of morphological texture, can offer valuable insights. Values approaching 1 signify ideal systems with well-established, long-range pathways between ionic clusters, while values below 0.5 indicate an ion-conductive network characterized by high tortuosity [39]. All membranes exhibit values near 1, indicating that the long-range pathways crucial for ion transfer remain unaltered.

To this respect, Fig. 12A reveals significant differences between membranes that use CYS and HMDA as curing agents, given that CYS-containing membranes have a T_v lower than T_g. Thus, the DGEBA/CYS and DGEBA/HMDA-CYS membranes exhibit three distinct zones: (i) a linear range from 313 to 363 K present only in cystamine-containing membranes; (ii) a non-linear region associated with cooperative motion of the membranes. Other studies on CANs with disulfide bonds, particularly those including CYS, have shown that the T_g lies between

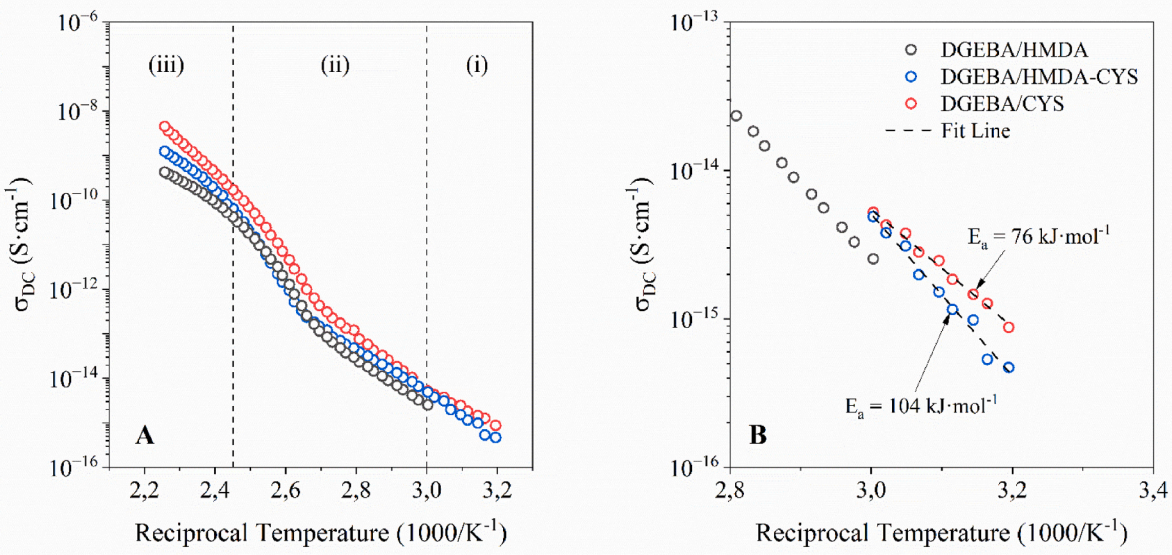

Fig. 12. (A) DC conductivity (σ_{DC}); (B) Detailed view of the DC conductivity for the DGEBA/CYS, DGEBA/HMDA, and DGEBA/HMDA-CYS membranes.

2.87 K^{-1} and 2.66 K^{-1} (348 K–375 K) depending on the CYS content [9, 10]; and (iii) a high-temperature linear zone attributed to electrode polarization.

In the case of the DGEBA/HDMA membrane only zones (ii) located between 2.4 and 3 K^{-1} (416 K–333 K) related to the glass transition, and (iii) due to the polarization of the electrodes are observed. Regarding the DGEBA/HMDA-CYS membrane, it displays the same three zones as the DGEBA/CYS membrane, but its behaviour falls within the range defined by the values defined by the DGEBA/HMDA and DGEBA/CYS membranes.

In Fig. 12B a detailed view of zone (i) is illustrated, which is attributable to the presence of disulfide bonds. As previously observed in Figs. 9 and 11, the characterization of zone (i) can provide insight on the underlying mechanism of the bond exchange reaction. An activation parameter of 76 kJ mol^{-1} falls within the plausible values for this exchange reaction, indicating that bond exchange reaction occurs in the range from 313 to 363 K which agrees with previous results [10].

Regarding the topological freezing temperature (T_v), three mechanisms have been proposed to govern the bond exchange reaction, as already shown in Scheme 1. Two with an associative nature (disulfide metathesis and thiol-disulfide exchange) and one with a dissociative nature (radical disulfide breakage). Covalent adaptable networks featuring an associative bond-breaking mechanism exhibit a σ_{DC} curve conforming to an Arrhenius model, as demonstrated in preceding studies. In contrast, networks with a dissociative bond exchange mechanism display a Vogel-Fulcher-Tamman-Hesse (VFTH)-like behaviour [18]. In Fig. 12B, region (i) exhibits complete linearity, implying that the bond exchange reaction has an associative nature. However, Figs. 9 and 11 show a significative increment in conductivity compatible with the presence of a radical-mediated exchange, that may be attributed to a dissociative bond exchange reaction. Nevertheless, these radicals rapidly form associations, and macroscopically, an associative behaviour is observed. Thus, these CYS-containing membranes exhibit a vitrimer-like behaviour. This is in accordance with previous results where the formation of radicals was detected through ESR analysis [11].

4. Conclusions

The analysis of the chemical structure of the membranes cured with three different systems (HMDA, CYS and an equimolecular mixture of HMDA and CYS) using DGEBA as epoxy resin, conducted through FTIR and Raman spectroscopy, confirmed that complete curing was achieved and that the expected functional groups were present.

An observable inverse correlation exists between the weight proportion of cystamine and the glass transition temperature. As the molar proportion of cystamine increased, the glass transition temperature decreased.

Dielectric spectra revealed three distinct dielectric relaxations labelled γ, β, and α, arranged in order of increasing temperature. Disulfide bonds caused changes in the dielectric spectrum. In the DGEBA/HMDA-CYS membrane, its relaxation function and activation energy are between those corresponding to the DGEBA/HMDA and DGEBA/CYS membranes, but their relationship does not depend linearly on the composition. In contrast, in the high-temperature region, the cleavage of disulfide bonds enhanced cooperative molecular motions and lowered the glass transition temperature.

The analysis of the electric conductivity (σ) reveals characteristic σ_{DC} curve of an associative bond exchange reaction. However, the abrupt increment in the electric conductivity of these membranes seems compatible with the presence of a radical-mediated exchange that may be attributed to a dissociative bond exchange reaction. Only the high speed in the formation of new associations of these radicals can explain that these CYS-containing membranes exhibit a vitrimer-like behaviour.

CRediT authorship contribution statement

B. Pascual-Jose: Writing – original draft, Visualization, Investigation, Formal analysis, Data curation. **R. Teruel-Juanes:** Visualization, Formal analysis, Data curation. **S. de la Flor:** Writing – original draft, Supervision, Resources, Investigation, Conceptualization. **A. Serra:** Writing – review & editing, Supervision, Resources, Investigation, Conceptualization. **A. Ribes-Greus:** Conceptualization, Formal Analysis, Funding Acquisition, Investigation, Project Administration, Supervision, Writing – Review & Editing. All authors have read and agreed to the published version of the manuscript.

Declaration of competing interest

The authors declare that they have no known competing financial interests or personal relationships that could have appeared to influence the work reported in this paper.

Acknowledgments

This study forms part of the Advanced Materials programme and was supported by the Spanish Ministry of Science and Innovation with funding from European Union NextGeneration EU (PRTR-C17.11) and by Generalitat Valenciana (MFA/2022/041). The authors also thank Universitat Politècnica de València for the grant PAID-10-23 SUB.1. The authors of the Universitat Rovira i Virgili would like to thank the funding of the projects TED2021-131102B-C22 and PID2023-147128OB-C22 provided by MCNI/AEI/https://doi.org/10.13039/501100011033 and European Union "NextGenerationEU"/PRTR. They also thank to the Generalitat de Catalunya (2021-SGR-00154).

Data availability

The data supporting the findings of this study cannot be shared at this time as the data also forms part of an ongoing study.

References

[1] R. Auvergne, S. Caillol, G. David, B. Boutevin, J.P. Pascault, Biobased thermosetting epoxy: present and future, Chem. Rev. 114 (2014) 1082–1115.
[2] F.L. Jin, X. Li, S.J. Park, Synthesis and application of epoxy resins: a review, J. Ind. Eng. Chem. 29 (2015) 1–11.
[3] Y. Yang, Y. Xu, Y. Ji, Y. Wei, Functional epoxy vitrimers and composites, Prog. Mater. Sci. 120 (2021) 100710.
[4] Z. Hu, et al., Efficient intrinsic self-healing epoxy acrylate formed from host-guest chemistry, Polymer (Guildf). 164 (2019) 79–85.
[5] Z. Hu, et al., Multistimuli-responsive intrinsic self-healing epoxy resin constructed by host-guest interactions, Macromolecules 51 (2018) 5294–5303.
[6] A. Ruiz De Luzuriaga, et al., Epoxy resin with exchangeable disulfide crosslinks to obtain reprocessable, repairable and recyclable fiber-reinforced thermoset composites, Mater. Horiz. 3 (2016) 241–247.
[7] M.A. Bin Rusayyis, J.M. Torkelson, Reprocessable covalent adaptable networks with excellent elevated-temperature creep resistance: facilitation by dynamic, dissociative bis(hindered amino) disulfide bonds, Polym. Chem. 12 (2021) 2760–2771.
[8] H.R. Khalafi, M. Ehsani, H.A. Khonakdar, Investigation of the cure kinetics and thermal stability of an epoxy system containing cystamine as curing agent, Polym. Adv. Technol. 32 (2021) 1251–1261.
[9] P. Verdugo, D. Santiago, S. De la Flor, À. Serra, A biobased epoxy vitrimer with dual relaxation mechanism: a promising material for renewable, reusable, and recyclable adhesives and composites, ACS Sustain. Chem. Eng. 12 (2024) 5965–5978.
[10] A. Roig, M. Agizza, À. Serra, S. De la Flor, Disulfide vitrimeric materials based on cystamine and diepoxy eugenol as bio-based monomers, Eur. Polym. J. 194 (2023).
[11] S. Nevejans, N. Ballard, J.I. Miranda, B. Reck, J.M. Asua, The underlying mechanisms for self-healing of poly(disulfide)s, Phys. Chem. Chem. Phys. 18 (2016) 27577–27583.
[12] Z.Q. Lei, H.P. Xiang, Y.J. Yuan, M.Z. Rong, M.Q. Zhang, Room-temperature self-healable and remoldable cross-linked polymer based on the dynamic exchange of disulfide bonds, Chem. Mater. 26 (2014) 2038–2046.
[13] J.M. Matxain, J.M. Asua, F. Ruipérez, Design of new disulfide-based organic compounds for the improvement of self-healing materials, Phys. Chem. Chem. Phys. 18 (2016) 1758–1770.
[14] K. Yamawake, M. Hayashi, The role of tertiary amines as internal catalysts for disulfide exchange in covalent adaptable networks, Polym. Chem. 14 (2023) 680–686.
[15] D. Montarnal, M. Capelot, F. Tournilhac, L. Leibler, Silica-like malleable materials from permanent organic, Networks 334 (2011) 965–968.
[16] B.R. Elling, W.R. Dichtel, Reprocessable cross-linked polymer networks: are associative exchange mechanisms desirable? ACS Cent. Sci. 6 (2020) 1488–1496.
[17] A. Ruiz de Luzuriaga, et al., Chemical control of the aromatic disulfide exchange kinetics for tailor-made epoxy vitrimers, Polymer (Guildf). 239 (2022) 124457.
[18] B. Pascual-Jose, S. De la Flor, A. Serra, A. Ribes-Greus, Analysis of poly (thiourethane) covalent adaptable network through Broadband dielectric spectroscopy, ACS Appl. Polym. Mater. 5 (2023) 1125–1134.
[19] F. Guerrero-Ruiz, I. Otaegi, E. Verde-Sesto, S. Bonardd, J. Maiz, Revealing dynamic behavior in high dielectric poly(thiourethane)-based vitrimer-like materials, ACS Appl. Polym. Mater. 6 (2024) 5473–5484.
[20] S. Kaiser, et al., The crucial role of external force in the estimation of the topology freezing transition temperature of vitrimers by elongational creep measurements, Polymer (Guildf). 204 (2020).
[21] F. Kremer, A. Schönhals, Broadband Dielectric Spectroscopy, Springer-Verlag Berlin Heidelberg, 2003.
[22] Q. Qin, G.B. McKenna, Correlation between dynamic fragility and glass transition temperature for different classes of glass forming liquids, J. Non-Cryst. Solids 352 (2006) 2977–2985.
[23] A. Cherdoud-Chihani, M. Mouzali, M.J.M. Abadie, Study of crosslinking acid copolymer/DGEBA systems by FTIR, J. Appl. Polym. Sci. 87 (2003) 2033–2051.
[24] H.E. Van Wart, A. Lewis, H.A. Scheraga, F.D. Saeva, Disulfide bond dihedral angles from Raman spectroscopy, Proc. Natl. Acad. Sci. U.S.A. 70 (1973) 2619–2623.
[25] D. Il Lee, S.H. Kim, D.S. Lee, Synthesis and characterization of healable waterborne polyurethanes with cystamine chain extenders, Molecules 24 (2019).
[26] S. Guggari, et al., Vanillin-based dual dynamic epoxy building block: a promising accelerator for disulfide vitrimers, Polym. Chem. (2024) 1347–1357.
[27] D.J. Fortman, R.L. Snyder, D.T. Sheppard, W.R. Dichtel, Rapidly reprocessable cross-linked polyhydroxyurethanes based on disulfide exchange, ACS Macro Lett. 7 (2018) 1226–1231.
[28] H.W. Starkweather, Noncooperative relaxations, Macromolecules 21 (1988) 1798–1802.
[29] H.W. Starkweather, Frequency-temperature relationships for relaxations in polymers, Thermochim. Acta 226 (1993) 1–5.
[30] R. Casalini, D. Fioretto, Influence of the glass transition on the secondary relaxation of an epoxy resin, Phys. Rev. B Condens. Matter 56 (1997) 3016–3021.
[31] I.A. Saeedi, N. Chalashkanov, L.A. Dissado, A.S. Vaughan, T. Andritsch, The nature of the gamma dielectric relaxation in diglycidyl ether Bisphenol-A (DGEBA) based epoxies, Polymer (Guildf). 249 (2022) 124861.
[32] J.D. Badia, et al., Dielectric spectroscopy of novel thiol-ene/epoxy thermosets obtained from allyl-modified hyperbranched poly(ethyleneimine) and diglycidylether of bisphenol A, Eur. Polym. J. 113 (2019) 98–106.
[33] E. do Nascimento, et al., Breakdown, free-volume and dielectric behavior of the nanodielectric coatings based on epoxy/metal oxides, J. Mater. Sci. Mater. Electron. 27 (2016) 9240–9254.
[34] S. Capaccioli, et al., Section 12. Polymer dynamics: dynamics of epoxies: a full dielectric analysis by wideband spectroscopy, J. Non-Cryst. Solids 235 (1998) 576–579, 237.
[35] W. Denissen, J.M. Winne, F.E. Du Prez, Vitrimers: permanent organic networks with glass-like fluidity, Chem. Sci. 7 (2016) 30–38.
[36] J.O. Simpson, S.A. Bidstrup, Rheological and dielectric changes during isothermal epoxy-amine cure, J. Polym. Sci., Part B: Polym. Phys. 33 (1995) 55–62.
[37] K. Friedrich, J. Ulanski, G. Boiteux, G. Seytre, Time-of-flight ion mobility measurements in epoxy-amine systems during curing, IEEE Trans. Dielectr. Electr. Insul. 8 (2001) 572–576.
[38] D. Krouse, Z. Guo, D.E. Kranbuehl, Isolating the mobility and characterizing the effect of crosslink structure versus the monomer state using ion time of flight, J. Non-Cryst. Solids 351 (2005) 2831–2834.
[39] K.A. Mauritz, H. Yun, Dielectric relaxation studies of ion motions in electrolyte-containing perfluorosulfonate ionomers. 3. ZnSO4 and CaCl2 systems, Macromolecules 22 (1989) 220–225.